Experimental study of the Alboran Sea gyres

Philippe GLEIZON, Gabriel CHABERT D'HIÈRES and Dominique RENOUARD

Laboratoire des Écoulements Géophysiques et Industriels - Institut de Mécanique de Grenoble (UJF-CNRS-INPG), BP 53 X, 38041 Grenoble Cedex, France.

ABSTRACT

In order to examine the response of the surface flow to the regime in the Gibraltar Strait, the Alboran Sea is modelled in a large rotating channel mounted on the 14 m "Coriolis" rotating platform. The channel is divided into two basins connected by a strait. The currents are initialized and maintained constant in time by pumps. When flowing out of the strait, the Atlantic current forms an anticyclonic gyre in the Mediterranean basin. This gyre is related to the Western Alboran Sea Gyre and can develop until its diameter is as large as the width of the basin. Depending on the parameters, the flow exhibits different configurations, which we are able to characterize with the use of tracers (food dye, floats). A very consistent result is that the flow seems to be deterministic, i.e. for the same initial and upstream conditions of stratification, rotation and flow rate, it shows the same pattern and the gyre evolves in the same manner. A parametric study shows that the characteristics of the gyre (shape, size, stability) are highly dependent on the ratio of the internal radius of deformation over the width of the strait, r/w, but not on the Rossby number, Ro, based on the flow rate of the currents. A meander, related to the Eastern Alboran Sea Gyre, can form downstream of the gyre. Its presence depends on r/w and also on Ro. A row of cyclonic vortices can develop along the frontal limit of the Atlantic jet.

The growth rate of the Gyre is determined by a flux budget analysis. The mechanism involved in this process was analysed by Whitehead (1985) and the experimental data supports his conclusions. We conclude that, whereas the internal radius of deformation plays a role in the structure and the stability of the Western Gyre, the flow rate of the Atlantic current influences the growth rate of the Gyre but does not change the flow drastically.

Finally, a comparison with the numerical simulation of Speich (1992) shows a fairly good agreement in spite of some minor differences.

RÉSUMÉ

Étude expérimentale des tourbillons de la Mer d'Alboran.

Dans la cuve tournante de 14 m de diamètre on installe un canal de 9 m de long, 2 m de large et 0,6 m de profondeur dans lequel on étudie l'écoulement de l'eau atlantique dans la Mer d'Alboran, les conditions d'apparition des tourbillons et leur dynamique. Le canal est constitué par deux bassins reliés par un détroit, et il est initialement rempli d'un bicouche eau douce – eau salée. Deux circuits hydrauliques indépendants permettent une circulation contrôlée dans chacune des couches. On mesure les champs de vitesses dans la couche supérieure ainsi que

le profil de l'interface entre les deux couches et on enregistre les différents types d'écoulements. Les paramètres du problème sont d'une part les débits dans le détroit et d'autre part le rapport entre le rayon interne de déformation dans le détroit et la largeur de celui-ci. Les résultats sont comparés tant avec les observations en mer qu'avec les modèles disponibles dans la littérature. L'écoulement dans le bassin est très déterministe et des conditions initiales et aux limites identiques produisent des écoulements similaires, seule diffère l'échelle de temps à laquelle ils peuvent être observés. L'étude paramétrique montre que les caractéristiques du tourbillon occidental ne dépendent pratiquement pas du nombre de Rossby Ro, mais du rapport entre le rayon interne de déformation dans le détroit et la largeur de celui-ci, r/w. À l'aval de ce premier tourbillon, on observe un tourbillon qui peut être associé au tourbillon oriental et qui serait alors le produit d'une instabilité du courant. La présence de ce dernier dépend des valeur de Ro et de r/w. De petits tourbillons cycloniques peuvent se développer le long du front entre l'eau atlantique et l'eau méditerranéenne. Les résultats expérimentaux sont comparés avec les études précédentes, en particulier de Whitehead and Miller (1979) et Whitehead (1985), et nos conclusions rejoignent celles de ces auteurs : le rayon interne de déformation dans le détroit joue un rôle important pour la structure et la stabilité du tourbillon occidental, et le débit d'eau atlantique influence son taux de croissance mais n'affecte pas la structure de l'écoulement. En dépit de différences de détail, on note un bon accord entre nos observations et les résultats des calculs numériques développés par Speich (1992).

INTRODUCTION

Both *in situ* measurements and satellite imagery clearly show that exchange flows occurring in straits can lead to the formation of large anticyclonic gyres in one of the adjacent seas. For instance, such a gyre is present off the Tsugaru Strait, between Hokkaido and Honshu Islands (Conlon, 1982), or again off the Bosphorus Strait when the lighter Black Sea water expands into the Marmara Sea (Betsiktepe *et al.*, 1990; Ünlüata *et al.*, 1990). However, the Alboran Sea Gyres are the most intensely studied examples of this phenomena. Lanoix (1974) was the first to depict this particular pattern; soon afterwards Gascard and Richez (1985) provided an exhaustive description of the flow between the Gulf of Cadix and the Alboran Sea. The temporal variability of the gyres was underlined by several authors (*e.g.* Cheney and Doblar, 1982; Perkins *et al.*, 1990; Heburn and La Violette, 1990); more recently, Le Vourch *et al.* (1992) presented a large amount of data and infrared thermograph pictures showing the characteristic patterns of the flow in the Alboran Sea and the Mediterranean. From these various studies it appears that the characteristic period of gyre variability is of the order of one month (Heburn and La Violette, 1990), while the e-folding time is about nine days (Perkins *et al.*, 1990). Moreover, a mesoscale turbulent activity is often superimposed on the mean flow. Perkins *et al.* (1990) found a cyclonic circulation developing between the western gyre and the Moroccan coast and Tintore *et al.* (1991) showed the presence of a row of cyclonic eddies in the front of the Atlantic jet. They suggested that this mesoscale turbulence can play an important role in the evolution with time of the western gyre. The cyclonic vortices measured by Tintore *et al.* (1991) can be related to the observation by Gascard

and Richez (1985) of patches of warm water in the Atlantic current which they consider as remnants of the Atlantic tides filtered by the strait. From hydrological data obtained by CTD measurements during October 1982, Perkins *et al.* (1990) estimated the inflow of Atlantic waters as approximately equal to 1.2 Sv (one Sverdrup -Sv- equals 10^6 m³/s), while the recirculating transport of the western gyre is O (1.5 Sv).

The gyre formation process has been analysed in several previous laboratory studies and modelled by numerical simulations. Whitehead and Miller (1979) defined the following four flow cases depending on the value of the internal radius of deformation, r, compared with the width (w = 10.2 cm), the length of the strait and the radii of curvature of the strait's corners at the outlet: (1) a strongly unstable flow for small radii of deformation (r < 3 cm); (2) weak instabilities for slightly higher values (3 cm < r < 6 cm) and a short strait; (3) a coastal jet for 6 cm < r < 8 cm or for a long strait, or also when the radius of curvature of the wall is larger or at least of the same order of magnitude as r; and (4) a gyre when r < 10 cm and with rather short radius of curvature. They showed that, for gyre formation, r must be larger than both the width of the strait and the radius of curvature of the corners. Bormans and Garrett (1989) extended these conclusions to the cases when the interface intersects the free surface. According to Klinger (1994), a baroclinic gyre forms downstream of a sharp corner if the angle of the walls is more than 45 degrees. Lastly, we should mention the parametric study made by Kawasaki and Sugimoto (1984). In their experiments, the gyre tends to form when the Rossby number has a value included between 0.5 and 1, and when the Ekman number is equal to 2.10^{-2}. Using a non-linear, semi-implicit, reduced gravity model, Preller and Hulburt (1982) made a sen-

sitivity study to estimate the influence of various parameters, finding that: (1) increasing the inflow angle gives a larger anticyclone; (2) the presence of negative relative vorticity in the inflow current induces a more pronounced leftwards deflection of the jet, as suggested by Nof (1978); (3) the width of the basin influences the gyre stability as well as the port location; and (4) the beta-effect enhances the development of the eastern meander. Another sensitivity study, carried out by Werner et al. (1988), obtains the same conclusions, except that these authors found no influence of the incoming negative relative vorticity upon the deflection of the Atlantic jet and that the beta-effect increases the size of the western gyre. In a recent work, Speich et al. (1994) use a 3D primitive equations model. The resulting simulation exhibits a realistic circulation of the water masses in the Alboran Sea.

In the present study, with the use of a large laboratory model, we evaluate more accurately how upstream conditions and geometric configurations influence the circulation in the Alboran Sea. In the following section, we present the model. Then the flow is described and characterized. It is studied in two different ways: (i) we shall characterize the flow by a global approach, i.e. a parametric study and an evaluation of the characteristic times; and (ii) a local study will be developed. We shall detail the various hydrodynamic processes which occur and show that together they can explain the global evolution and structure of the gyres. Finally, we conclude with a discussion and a comparison with the Alboran Sea flow and with the numerical model of Speich et al. (1994).

Parameters of the problem and physical modelling

According to Gascard and Richez (1985), the flow in the Gibraltar Strait and the Alboran Sea can be regarded as a two-layer system, where the interface is located at the isopycnals of $\approx$ 28 to 28.5. Thus, the physical model uses a two-layer system. From previous studies, it appears that the parameters playing a role are: the geometrical dimensions,

length l width w and depth d of the strait, and the width W and depth D of the basin; the reduced gravity g'; the background rotation represented by the Coriolis parameter f; the thickness of the upstream upper layer h_u (the related thickness of the upper layer in nature is taken over the Camarinal Sill); the flow rates of the two currents, Q_1 and Q_2 in the upper and lower layers respectively; the mean flux velocity of these currents, U_1 and U_2; and the horizontal and vertical kinematic viscosity, respectively u_h and u_v. Indeed, some of these parameters are linked for: $Qi = Uidw/2$ where the subscript $i = 1,2$ denotes the upper ($i = 1$) and lower ($i = 2$) layers, respectively. Thus, ten non-dimensional numbers should be necessary to model this flow. However, for this set of experiments, the scale parameters d/D, w/l, d/w and D/W are constant and in similitude with the Gibraltar Strait and the Alboran Sea. However, the model is distorted vertically by a factor of 30 (ratio of vertical to horizontal scale) to set the Ekman number in a compatible range with nature. As a consequence, the distortion inhibits the bottom friction with respect to the other phenomena. Since the eddy kinematic viscosity in nature is not clearly defined, the Ekman numbers v_h/fw^2 and v_v/fd^2 can hardly be used in the scaling. We only check that they are included in the same range of values as those estimated by Pedlosky (1987, p.185). The flux ratio Q_1/Q_2 is constant and the same for all experiments $Q_1/Q_2 = 1$. Thus, the similitude and the parametric study can be done with only three non-dimensional numbers:

(1) $B = r/w$, which is the ratio of the internal Rossby radius of deformation $r = (g'h_e)^{1/2}/f$ over the width of the strait, where $h = h_u(D - h_u)/D$;

(2) $Ro = U_1/fw = 2Q_1/fdw^2$, the Rossby number of the Atlantic inflow;

(3) $\eta = h_u/d$, the non-dimensional upstream upper layer thickness. The values of the characteristic parameters and non-dimensional numbers for all the experiments considered here are listed in Table 1.

We use the 14 m diameter rotating platform equipped with a 9 m long, 2 m wide and 0.6 m deep channel which is divided into two basins connected by a strait (Fig. 1). A

Table 1

Characteristics of the experiments. B is considered as a Burger number $B = r/w$ where r is the internal radius of deformation and w the width of the strait. Ro is the Rossby number of the Atlantic current $Ro = 2Q/fdw^2$. η is the upstream non-dimensional thickness $\eta = h_u/d$. A quantitative information means that the velocity field and the interface topography are determined on a regular 10 cm spaced grid.

Run	Dimensional parameters				Non-dimensional numbers			Information
	$f (s^{-1})$	$g' (cm/s^2)$	h_u (cm)	$Q (cm^3/s)$	B	Ro	η	
1	0.167	1.765	7.5	270	0.8	0.47	0.68	food dye
2	0.12	2.65	7.5	270	1.2	0.65	0.68	food dye
3	0.16	1.67	7.5	200	0.8	0.37	0.68	trajectories
4	0.135	2.55	7.5	270	1.2	0.58	0.68	trajectories
5	0.126	2.84	5.5	200	1.2	0.46	0.5	trajectories
6	0.12	2.55	5.5	200	1.2	0.48	0.5	trajectories
7	0.14	2	13	100	1.2	0.94	1.18	quantitative
8	0.17	2.35	5.5	160	0.8	0.27	0.5	trajectories
9	0.21	2.45	7.5	125	0.76	0.17	0.68	quantitative
Alb.Sea	8.5×10^{-5}	1.96	2×10^4	1.2×10^{12}	0.8 to 1	≈ 0.24	0.66	

Figure 1

Sketch of the experimental facility.

L=9 m
W=2 m
D=0.55 m
l=0.75 m
w=0.25 m
d=0.11 m

hydraulic system of sources and sinks ensures a permanent circulation of the water in each layer. The upper-layer current is supplied by a constant discharge of fresh water in the smallest basin, referred hereafter as the "Atlantic" basin, and removed via a sink in the largest basin, the "Mediterranean" basin. Conversely, the motion in the lower (salted) layer water is induced by a sink in the Atlantic basin and a source in the Mediterranean basin which are connected through a constant discharge pump (Fig. 1). Thus, the flow in the Gibraltar Strait and in the Alboran Sea is modelled by a two-layer system and we can adjust the volume flow rate in each layer. We note by x and y respectively the along- and across-basin directions, the origin being located at the "southwestern" corner of the Mediterranean basin (Fig. 1).

The flow pattern is monitored by dye tracers and float trajectories, and we use visualization techniques to measure the velocity field and interface depth. The surface velocity field is obtained by following a large number of floats. Photographs are taken during a brief period (15 s) which is long enough to minimize measurement errors but much shorter than the characteristic evolution time of the flow. Thus, as we obtain short parts of the trajectory, the deduced lagrangian velocity can be assimilated to eulerian velocity. The velocity field is interpolated on a mesh grid, with a 10 cm step, using the Adaptive Gaussian Windows Method (Agui and Jimenez, 1987). Each vector is calculated by looking at the closest measured values and averaged with a weighting function α (r):

$$\bar{u}(i,j) = \sum_{x,y} \bar{u}(x,y)\alpha(r) / \sum_{x,y} a(r),$$

where $\alpha(r) = \exp\{-(2r/R)^2\}$, $r^2 = (x-i)^2 + (y-j)^2$ and R = 10 cm (mesh-grid step), (x, y) being the co-ordinates of the point where the velocities are measured, and (i, j) the co-ordinates of the positions of the interpolated vectors on the mesh grid. The floats also provide a good visualization of the flow by their trajectories. These methods allow us to observe the general flow pattern and to collect accurate data.

Consequently, we are able to perform a parametric as well as a process study. The interface depth is measured by using a vertical laser sheet perpendicular to the x-direction (Fig. 2). The upper layer is differentiated from the lower layer by adding a fluorescent dye. A video camera records the images, which are analysed and corrected in order to measure the depth of the interface. The measurement errors are O (10 %). This method only gives data in one cross-section. The acquisition is repeated many times to obtain the entire interface field in the Mediterranean basin. Due to the large scale of the experiment, a series of acquisitions can take a long time. In the worse case, the period of acquisition is in the same range as the time of evolution of the gyre.
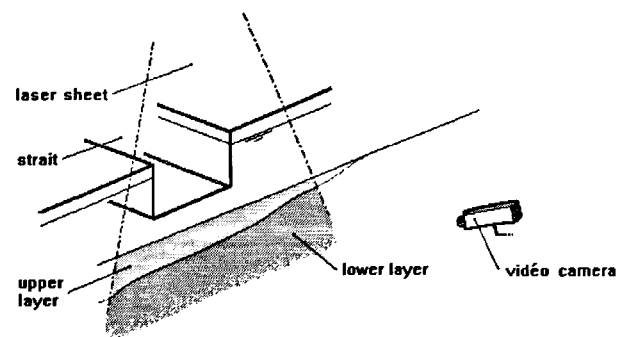
Figure 2

Sketch of the measurement system of interfacial depth. Fluorescent dye is added to the dense water (lower layer) to make it distinguishable from the light water (upper layer). The laser sheet can move along the channel to collect information on the whole basin. The recorded image is analysed to correct perspective and refraction errors.

General flow description and parametric study

All observations with dye or float trajectories show that the Atlantic jet of light water is deflected to the right as it moves out of the strait and generates a gyre which then grows, fed by incorporating part of the incoming Atlantic
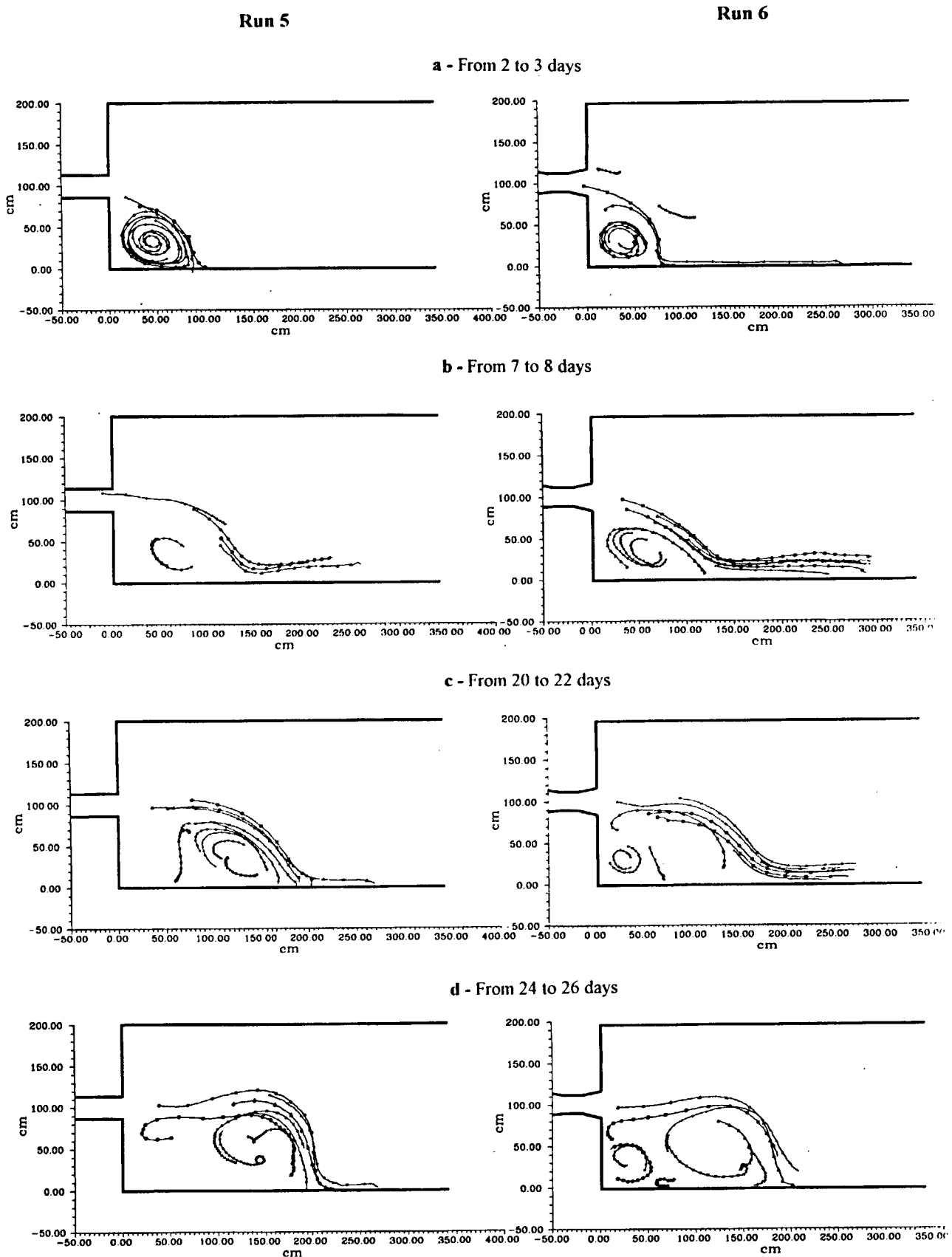
Run 5   **Run 6**

a - From 2 to 3 days

b - From 7 to 8 days

c - From 20 to 22 days

d - From 24 to 26 days

Figure 3

Comparison of the flow evolution for runs 5 and 6. The trajectories are obtained at four different times. The time interval between two dots is 10 s.

jet when the latter hits the wall (coast). The pattern follo-wed by the flow is very deterministic, *i.e.* the flow is reproducible for the same given conditions. Figure 3 pro-vides an example of two runs for which the parameters are similar. The trajectories are compared at four different times from the beginning of the experiments. While some

trajectories are lacking as, for instance, in the "southwestern" corner of the basin for run 5 after 20 days, there are strong similarities in the evolution of the two flows. Also, one can note that this similarity occurs despite a slightly different strait geometry: in run 5, the width of the strait is constant at 25 cm, while in run 6 it is progressively variable from 25 cm in the centre of the strait to 35 cm at the outlets. Hence the shape of the strait has no significant influence on the gyre formation, and the flow pattern in the basin is linked to the parameters in a deterministic sense. Thus, we can classify the flows in two distinct categories according to the hydrodynamic conditions: (i) unstable gyre; and (ii) stable gyre, as illustrated in Figure 4. The former case is characterized by a small gyre which forms quickly and detaches from the mean current before growing and progressively occupying the whole basin width (Fig. 4*a*). After the gyre separates from the current, the Atlantic current follows the wall (coast) before a second gyre begins to form again at the outlet of the strait and the process repeats itself. The latter case is characterized by a more stable gyre which is always surrounded by the Atlantic current and grows regularly until its size is limited by the width of the basin (Fig. 4*b*). This latter case is closer to the Alboran Sea flow configuration.

The surface flow in the Alboran Sea shows other features. Such as a second anticyclonic gyre which appears in the eastern part of the basin. In some experiments, a meander of the coastal current downstream of the gyre develops and gives rise to an anticyclonic circulation which is related to the eastern gyre. Figure 5 shows, together with the surface velocity field (Fig. 5*a*) and the interface topography (Fig. 5*b*), the presence of a meander at x = 4 m, larger

than the anticyclonic gyre. The reason why such a phenomenon occurs can be related to the instability process in a coastal current (Chabert d'Hières *et al.*, 1990; Obaton, 1994). We mentioned previously a mesoscale activity in the Alboran Sea. In some experiments, a row of cyclonic vortices appears along the front of the Atlantic current (Fig. 6). As shown in the scheme of Figure 6*b*, they appear when: (i) the gyre is fully developed, *i.e.* when it occupies the whole width of the basin so that the Atlantic current surrounding it encounters the wall related to Spanish coasts; and (ii) B < 1. Finally, a cyclonic vortex forms during all experiments in the corner between the walls related to the southwestern part of the Moroccan coast and the gyre. In Figure 6, this eddy is marked by red dye and appears as a dark spot on the picture.

Depending on the parameter values, the flow exhibits various characteristic patterns. When the gyre starts growing, its radius is B-dependent, as illustrated in Figure 7. The pictures come from the two different experiments, but are taken at the same time after the beginning of the run. In Figure 7*a* (run 1), where B = 0.8 and Ro = 0.47, the radius of the gyre is smaller than in Figure 7*b* (run 2), where B = 1.2 and Ro = 0.65. In the same fashion, the two markedly different structures of the "western" gyre, depicted above (Fig. 4), can be plotted as function of B and Ro. The unstable gyres occur only for small B, at least B < 1. But the flow type does not depend on Ro, which means that the volume fluxes through the strait have little influence on the structure of the gyre. For the occurrence of the meander referred to earlier as the "eastern gyre", we observe three distinct cases: (i) the absence of the meander; (ii) a weak and ephemeral meander; and (iii) a strong, persistent and
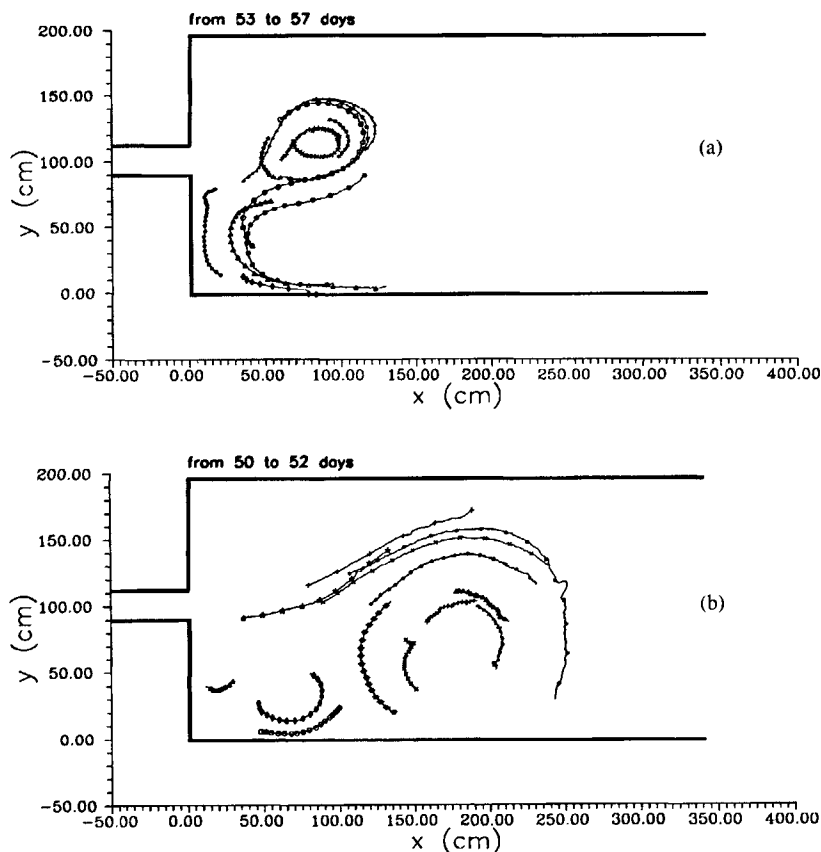

(a)

from 53 to 57 days

(b)

from 50 to 52 days

Figure 4

Example of typical flows of (a) unstable gyre (run 3) and (b) stable gyre (run 4).
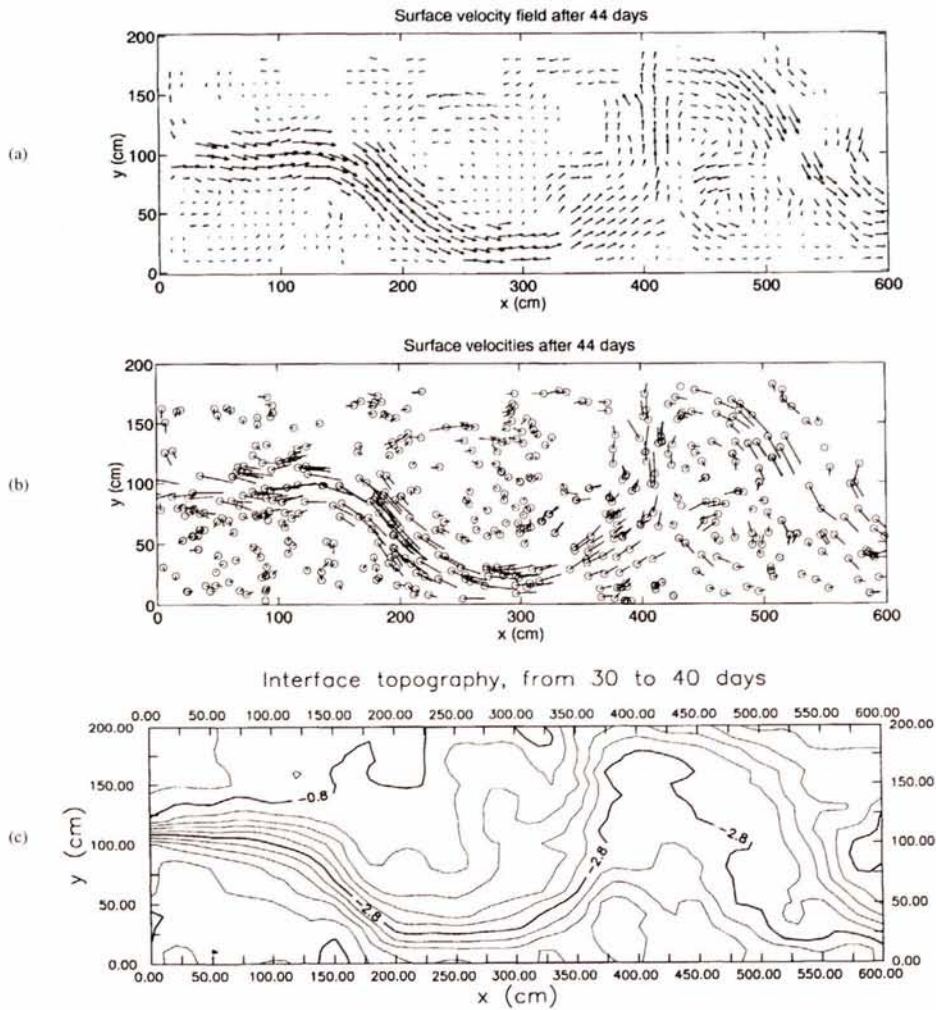
Figure 5

Surface flow during run 7. (a) Velocity field interpolated on a grid from the (b) advection of floats randomly arranged and (c) interface topography. The strong correspondance between the graphs indicates that the flow is in geostrophic equilibrium. The wavelike pattern of the flow exhibits a weak western gyre at $x \leq 200$ cm and $y \leq 80$ cm, and a large meander related to the eastern gyre at $400 \leq x \leq 520$ cm and $y \leq 150$ cm.
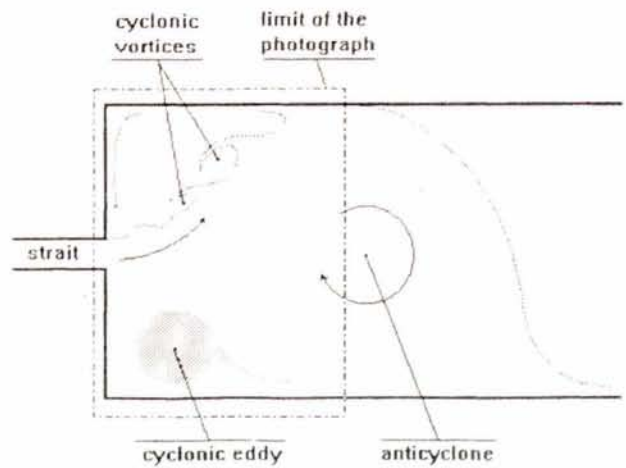

Figure 6

Formation of a row of cyclonic vortices along the front of the Atlantic jet. The strait is located on the left side of the photograph, while the gyre is on the right side. The vortices are marked by green dye surrounded by red dye (limit of the front). The frontal disturbance is perceptible in the wavelike motion of the current near the strait. The red spot in the left-bottom indicates a cyclonic eddy formed by the influence of the gyre on the angle of the basin.
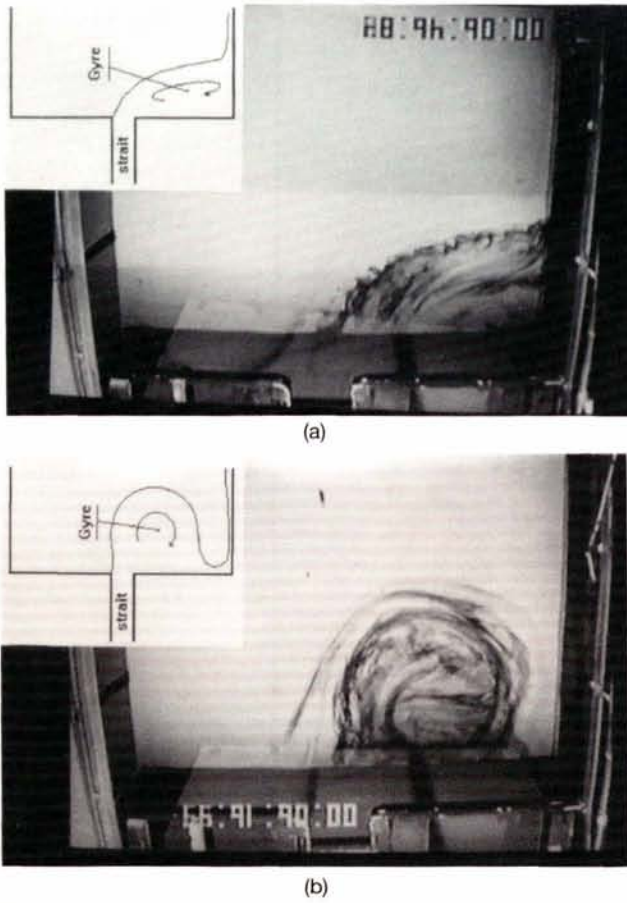
(a)

(b)

Figure 7

Formation of the gyre for (a) B = 0.8 (run 1) and (b) B = 1.2 (run 2).

well-formed meander. These three cases are plotted in function of B and Ro (Fig. 9). For B < 1, the "western gyre" is unstable and the "eastern gyre" non-existent. This case is far from the observations in the Alboran Sea. For B ≥ 1, the "western gyre" is stable and the "eastern gyre" can form when B ≈ 1.2 and Ro > 0.3. In this case, the flow pat-
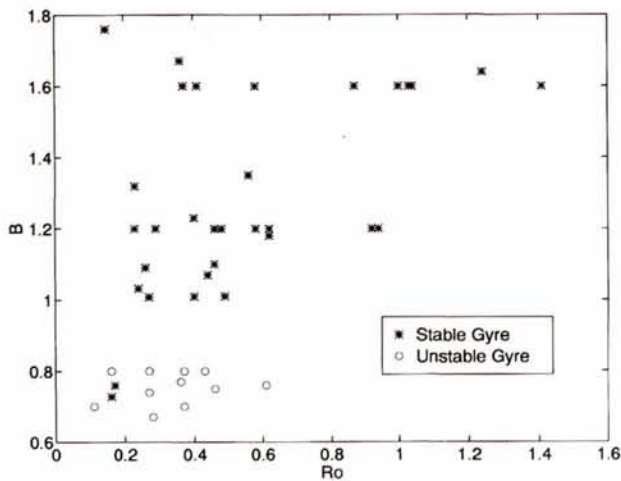

Figure 8

Stability diagram of the western gyre as function of the Burger number B = $\sqrt{g'h_e}/fw$ and the Rossby number Ro = $2Q/fdw^2$. The open circles are related to unstable gyres (Fig. 4a), the stars to the stable gyres (Fig. 4b).
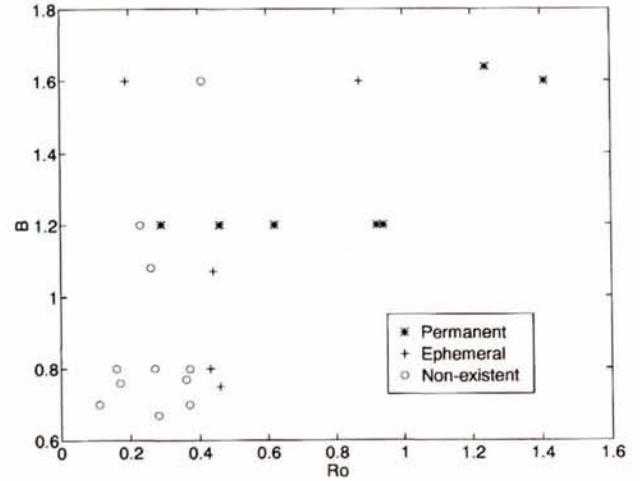

Figure 9

Stability diagram of the presence of the eastern gyre as function of the Burger number B = $\sqrt{g'h_e}/fw$ and the Rossby number Ro = $2Q/fdw^2$.

terns exhibit a rather good similarity with the observed surface flow in the Alboran Sea. Figure 5 belongs to this latter case, with B = 1.2 and Ro = 0.94. In the Strait of Gibraltar and the Alboran Sea, B varies in the range [0.8-1.2] (Gascard and Richez, 1988), and Ro ≈ 0.25. Thus, from our set of experiments, both gyres may or may not be present.

Process study

From the above observations, it is evident that the growth rate of the "western gyre" is related to the recirculating flux of the "Atlantic jet". With the objective of an application to the Alboran Sea gyres, Whitehead (1985) studied the deflection of a baroclinic jet by a wall. He showed that the flow rate and the momentum of the recirculating branch of the jet depends on the incidence of the jet to the wall. We keep the same notations as Whitehead (1985). Let us consider Figure 10. Let η be the perpendicular to the streamwise direction of the impinging jet, and θ the angle of the jet *versus* the normal of the wall, directed positively
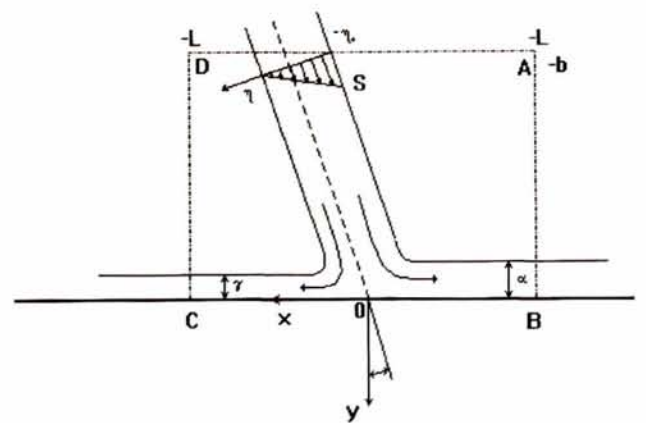

Figure 10

Sketch of the deflection of the Atlantic baroclinic jet by the wall.

506

in the trigonometric sense. The widths of the two branches of the jet are γ (recirculating branch) and α (evacuating branch), as depicted in Figure 10. The assumptions are no viscous effects, geostrophic equilibrium and conservation of the potential vorticity. Whitehead (1985) distinguishes two cases: (i) zero potential vorticity; and (ii) constant (but non-zero) potential vorticity. For each case, the velocity (S) and the thickness (h) of the jet are determined in function of η. They are, for case (i): S = -fη and h = H - $f^2\eta^2/2g'$, where H is the upper layer thickness when $\eta \to \infty$, i.e. it represents the mean depth of the interface under the gyre. The width of the jet is defined as $\eta_0 = (2g'H)^{1/2}/f$. For case (ii): S = $(g'H)^{1/2}$ exp[-η/η_0 + 1)] and h = H{1 - exp[-η/η_0 + 1)]}, with $\eta_0 = (g'H)^{1/2}/f$. Integrating the momentum equations on the contour ABCD (cf. Fig. 10) gives a relation between θ and the non-dimensional width of the recirculating branch $\lambda = \gamma/\eta_0$. In case (i), $5\lambda^3 - 3\lambda^5 - 1 + \sin(\theta) = 0$ and in case (ii), $4e^{3(\lambda-1)} -6e^{3(\lambda-1)+1} - \sin(\theta) = 0$.

The integrated volume flux of the recirculating branch is, for case (i):

$$Q_r = \lambda^2 (2 - \lambda^2) \qquad (1)$$

and for case (ii):

$$Q_r = 1 - 2e^{(\lambda-1)} + e^{2(\lambda-1)} \qquad (2)$$

From the velocity and the interface depth fields, we are able to determine the angle of incidence of the jet at the wall and to compute roughly the flow rate in each branch. As shown, as an example, in Figure 6 by the velocity field and the interface topography of run 6, we are able to prove that, in first approximation, the flow is in geostrophic equilibrium. We can assume that the effects of viscosity are negligible. The measured percentage of evacuated flux (to the right in Figure 10) is compared with the theoretical curves found by Whitehead (1985), in Figure 11. This comparison, which has been made for the runs where both the measurements of velocity and interface depths are good enough, shows a good agreement with the predictions. Unfortunately, the velocity field is interpolated on a 10 cm mesh grid, while the current width is of order of 40 cm. Thus, the calculation has a poor resolution and it is not possible to say whether the flow is closer to case (i) (zero potential vorticity) or to case (ii) (constant potential vorticity).

We assume that the growth rate of the gyre depends on the flow rate of the recirculating fluid. The characteristic time of evolution $\mathcal{T}$ is defined as the ratio of the fluid volume $\mathcal{V}$ of the gyre to its temporal variation

$$\mathcal{T} = \mathcal{V}\left(\frac{\partial \mathcal{V}}{\partial t}\right)^{-1} \qquad (3)$$

and $\mathcal{V}(t)$ can be interpreted as the time integrated net recirculating flux: $\mathcal{V}(t) = V \int_0^t (Q_1 - Q_1'(\tau)) \, d\tau$ where Q_1 is the flow rate of the upper layer in the strait and Q_1' the evacuated flux, as presented in Figure 12. In an experiment, Q_1 is constant but Q_1' can vary depending on the inclination of the jet with regard to the wall. For example, we estimate the volume of water of the "western gyre" in Figure 6: $\mathcal{V} \approx 60$ l. The net volume flux is: $(Q_1 - Q_1') \approx 2.4$ l/min. Thus, for this example, $\mathcal{T} \approx 25$ min. An experiment duration is 90 to 120 min. Note that $\mathcal{T}$ increases during the experiment, since $\mathcal{V}$ increases. As mentioned previously, the flow develops in the same way for equivalent experiments (with the same Burger number B). Let us consider
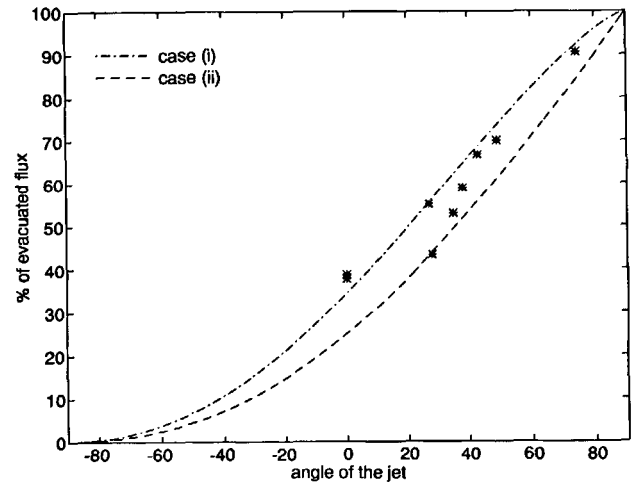

Figure 11

Percentage of the evacuated flux Q_r (flowing on the right on the Figure 10) versus the angle θ of the jet and comparison with the theory of Whitehead (1985). The curves indicate the theoretical percentage for cases of zero potential vorticity (case (i)) and constant potential vorticity (case (ii)). The stars are the measured values.

two similar runs with different flow rates Q_1. Let $t^{(1)}$ and $t^{(2)}$ be the real times for which the two flows exhibit the same patterns, and $\mathcal{T}^{(1)}$ and $\mathcal{V}^{(2)}$ the characteristic times of evolution as defined in eq. (3). As the patterns are identical, $\mathcal{V}$ follows the same evolution. We can also assume the percentages of recirculating fluid to be the same. The same phenomena may be expected to occur during the same non-dimensional time, say for: $t^{(1)} / \mathcal{T}^{(1)} = t^{(2)} / \mathcal{T}^{(2)}$. Thus, the non-dimensioning of the time is conversely proportional to the flow rate: $t^{(1)} / t^{(2)} = \mathcal{T}^{(1)} / \mathcal{T}^{(2)} \propto Q_1 / Q_2$. It seems correct to non-dimension the actual time by a time scale based on the flux of the upper current in the strait:

$$T = wh_u l / Q_1 \qquad (4)$$

The best illustration of the choice of the temporal non-dimensioning is given by the comparison of runs 8 and 9 (Fig. 13). These two experiments have close but slightly different characteristics. In particular, for both experiments, B $\approx$ 0.8. But the flow rates are respectively for runs 8 and 9, 160 cm^3/s and 125 cm^3/s. Figure 13 represents
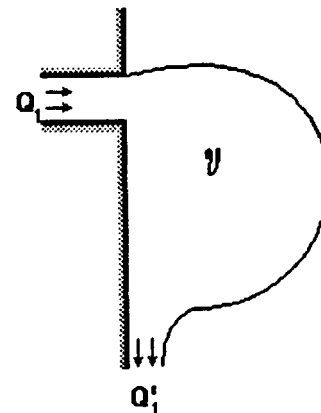

Figure 12

Diagram of flux distribution. Q_1 is the flux of the Atlantic current in the strait, Q_1' the flux of the coastal current, and $\mathcal{V}$ the volume of the gyre.
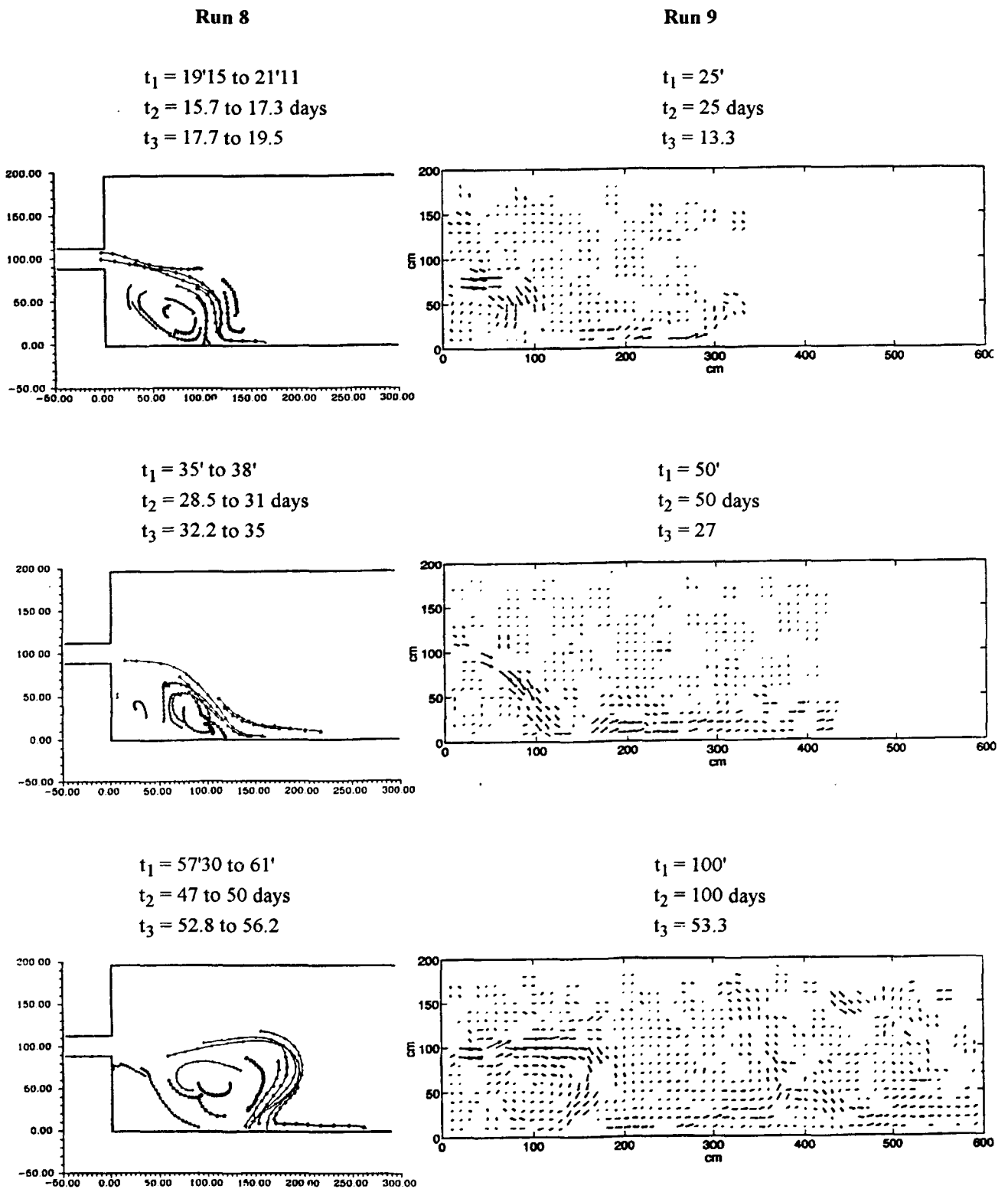
Run 8

$t_1 = 19'15$ to $21'11$

$t_2 = 15.7$ to 17.3 days

$t_3 = 17.7$ to 19.5

Run 9

$t_1 = 25'$

$t_2 = 25$ days

$t_3 = 13.3$

$t_1 = 35'$ to $38'$

$t_2 = 28.5$ to 31 days

$t_3 = 32.2$ to 35

$t_1 = 50'$

$t_2 = 50$ days

$t_3 = 27$

$t_1 = 57'30$ to $61'$

$t_2 = 47$ to 50 days

$t_3 = 52.8$ to 56.2

$t_1 = 100'$

$t_2 = 100$ days

$t_3 = 53.3$

Figure 13

Comparison of the flow evolution of runs 8 and 9 for which B is the same (B ≈ 0.8) and the flow rate of the Atlantic current is slightly different ($R_0 = 0.27$ for run 8; $R_0 = 0.17$ for run 9). Both runs exhibit the same evolution but for different runs. t_1 is the experimental real time; t_2 is the time non-dimensionalized by the background rotation period $t_2 = ft/4\pi$; t_3 is the time non-dimensionalized by the advection period $t_3 = tQ/wh_u d$.

three stages (plotted on the lines) of the two flows (plotted on the columns). For each case, the different times are indicated as following: $t_1 = t$ actual time, $t_2 = t/T$ where T is the background rotation period, and $t_3 = t/T$. In spite of different techniques of measurements, the flows develop in

strikingly the same fashion. Looking at the three stages represented in Figure 13, we notice that the same flow patterns do not occur at the same real time. A non-dimensioning using T increases the discrepancy of the time, while a non-dimensioning using T gives a better correspondence.

508

Careful attention must be paid when one tries to compare different models or to obtain an application to the natural flow. It is more convenient to scale the time with the background rotation period since, for mesoscale flows (length scale ~ O (100 km) in the oceans), the Coriolis parameter f can be regarded as an invariant. The development of the Alboran Sea western gyre is correctly reproduced when the non-dimensional numbers are in similitude. Indeed, as shown by Figure 13, the evolution of the flow is well represented by the non-dimensional time $t_3 = Q1t/wh_u1$. If the related time is $t_2 = t/T$, then the evolution of the flows are similar when t_2 is proportional to t_3, say $t_2 = Kt_3$ where K is a constant and must be the same for the related flows. From the above expressions of t_2 and t_3, we find K to be a function of Ro, h and geometrical parameters: K = η/Ro. $1/2\pi w$. In consequence, the evolution of the flows can be compared using a time non-dimensioned by the background rotation if the flows are in similitude in Ro, η and l/w (or at least in similitude in η/Ro. l/w). One of the difficulties in the comparison between models and the natural flow stems from the variation of fluxes in the strait depending on meteorological conditions and tidal fluctuations.

DISCUSSION

The most striking feature exhibited by this set of experiments is the highly deterministic behaviour of the flow in the Alboran Sea as a function of the upstream parameters in the strait. First, it appears that the volume flow rate in the strait influences the growth rate of the gyre but not its general structure; for instance, in runs 8 and 9, which differ only in the volume flow rate, we observe the same pattern although with a temporal phase shift: the larger the volume flow rate, the faster the gyre develops. Second, it appears clearly that the observed pattern is strongly related to the ratio of the internal radius of deformation in the strait to the strait width. In the Gibraltar Strait, such variations are related to the hydrological variations of the density difference between the inflow and the outflow. According to Gascard and Richez (1985), the internal radius of deformation varies in the range [16.5 - 19.5 km], so that B = R/w is in the range [0.8 - 1] since w = 20 km. This result is in agreement with Whitehead and Miller (1979) and Conlon (1982), suggesting that the variability of the flow pattern is correlated with the variations of the internal radius of deformation. The main difference between their experiments and ours is that in the latter, the flow is induced thanks to a hydraulic system, whereas in the former the Rossby adjustment was used. The present set of experiments allows for a better control of the current discharge, which is set constant at a chosen value throughout the experiment, thus ensuring controlled time-independent boundary conditions. From satellite images gathered in 1982, 1985 and 1986, Heburn and La Violette (1990) characterize the presence or the absence of the Alboran Gyres: the western gyre is principally absent in spring (March to May) and present in summer (August) and winter (December and January). Between January and March, there is

deep water formation and homogenization of the water column and thus a reduction of the density gradient. This can explain the decrease of the internal radius of deformation in the strait, and consequently the change in behaviour of the gyres. For if the internal radius of deformation decreases, the flow evolves into an unstable gyre or equivalently into a coastal jet, in agreement with the observations of Whitehead and Miller (1979). Conversely, an increase of the internal radius of deformation leads to the formation and growth of the western gyre.

The reason for the existence of the eastern gyre is not clearly understood. Some of our experiments show the development of a large anticyclonic circulation related to the eastern gyre. This circulation seems to be dependent on the Burger number B (and thus on the internal radius of deformation) and, less obviously, on the Rossby number Ro. The occurrence of this gyre strongly depends on the presence and development of the western gyre. The eastern gyre can be seen as a consequence of the destabilizing effect of the baroclinic jet on the subsequent coastal current, as in the case of the Algerian current, when several successive meanders develop along the coast (Obaton, 1994). Preller and Hulburt (1982) suggested that the meandering current in the western part of the sea might be considered as a standing Rossby wave, due to beta-effect. However, our physical model represents only schematically the actual Alboran Sea, since the Tres Forcas Cape and the topography are not reproduced. Thus, the development and growth of the meander with such a simple geometry suggests the minor importance of such topographical or coastal effects. The beta-effect is, therefore, probably not the most influential factor for the start of the meandering, although it may have some influence after the meander appears. Using a more realistic schematization of the Alboran Sea, Whitehead and Miller (1979) show that the western gyre remains located in the western part of the sea, west of Cape Tres Forcas. This corroborates the observations of several authors (Lanoix, 1974; Perkins et al., 1990; Le Vourch et al., 1992). Following Whitehead (1985), the growth rate of the gyre can be correlated with the flow rate of the recirculating part of the Atlantic Jet, after it impinges on the African coast and splits into two branches. The variation of that flow rate is due either to variations in the incoming flux of Atlantic water through the strait, or to a change in the incidence of the jet with respect to the African coast. The presence of Cape Tres Forcas, which is located where the jet meets the coast, can probably influence the flux balance between the two branches. If the jet impinges on the coast beyond the cape, the flow rate of the two recirculating branches strongly decreases, inducing a rapid decrease in the gyre growth. Furthermore, it is interesting to compare our observations with the jet model developed by Nof (1978) showing that the baroclinic jet can deflect to its left by geostrophic adjustment, for instance in the case when the Atlantic current in the strait has a negative relative vorticity of at least the same order as the Coriolis parameter. The velocity profiles of the upper-layer current measured in the strait reveal an anticyclonic relative vorticity (Gleizon, 1994). We tried to relate the vorticity computed from this measurement to the direction of the Atlantic jet. For various

experiments, we determine the angle of incidence θ_0 the jet takes at its entrance in the basin, and plot it versus the non-dimensional relative vorticity of the Atlantic current - $(\partial u_1/\partial y)f$ (Fig. 14). No obvious relation appears between the two phenomena, but this does not invalidate Nof's theory since, in our model, the negative relative vorticity is always much less than the Coriolis parameter. Thus, the observed jet deflection, as shown on the trajectories of Figure 4, is probably less linked to a geostrophic adjustment of the baroclinic jet than to the internal dynamics of the gyre which introduces a pressure gradient perpendicular to the incoming jet direction.

An interesting comparison can be made with the numerical simulation of Speich (1992). Some features observed in the experiments have been found in the simulation. For instance, the simulation reproduces the formation and the growth of the western gyre with a rather good similarity. The most striking likeness is given by Figure 15. The graphs plotted on this figure represent the velocity fields of (a) numerical and (b) experimental simulations which are in similitude ($B_{num} = 0.75$ and $B_{exp} = 0.76$). The two patterns are close in the sense that the sizes of the gyres are identical, the Atlantic current follows the same path: it is stretched when flowing out of the strait, and then deflects on its right and arrives at the wall with the same angle before separating into two branches. The left branch (looking streamwise) gives way to a coastal current. However, the flow appears more variable in the experiment than in the simulation. This observation (not shown) can explain the temporal difference between the flow patterns of Figure 15, whatever the non-dimensioning of time is. Both models show: (i) the deflection of the Atlantic jet; (ii) the formation of cyclonic eddies on the frontal limit of the Atlantic jet; (iii) the appearance of the eastern anticyclonic gyre; and (iv) an anticyclonic circulation in the dense water, related to Western Mediterranean Deep Water (WMDW), under the western gyre.
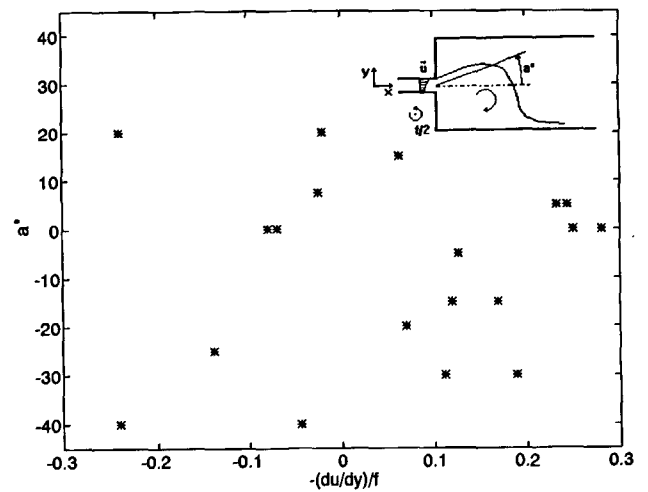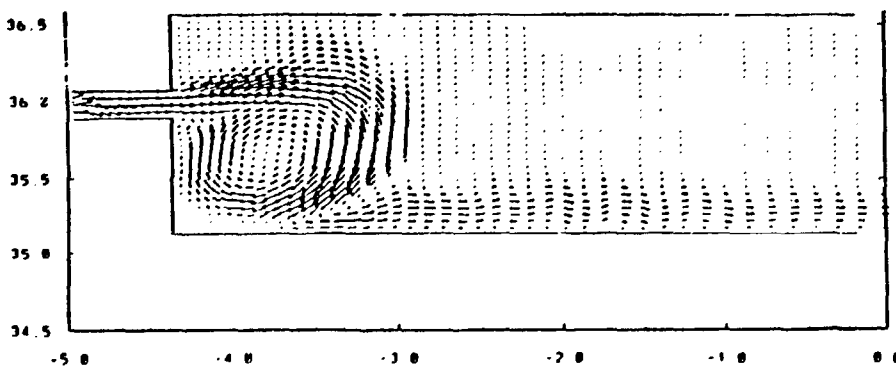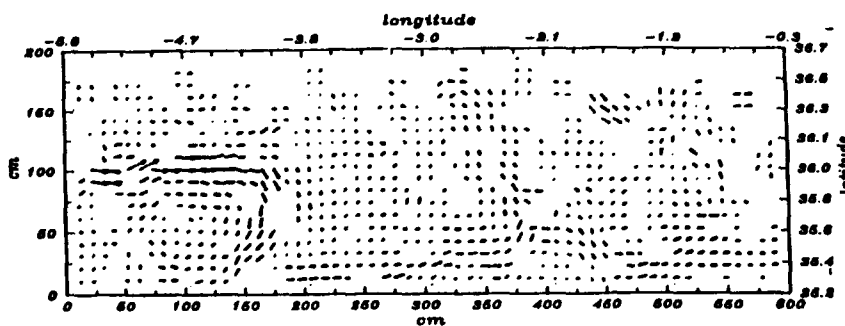

Figure 14

Influence of the negative relative vorticity of the Atlantic current on the deflection of the jet.

The deflection of the Atlantic jet is an effect of the internal dynamics in the basin, associated with the growth of the western gyre, as observed on both models. A slight difference is noticeable in the structure and the cause of the cyclonic eddies in the north of the gyre. In the numerical simulation, the cyclonic eddies have a diameter of 50 to 75 km, *i.e.* at least one-third of the width of the basin or half the diameter of the anticyclonic gyre. Speich (1992) noted that this eddy is filled by dense water and considered that it is generated by barotropic effects. In the experiments, a row of cyclonic vortices has been observed along the front of the Atlantic jet (Fig. 7). They occur under particular conditions: the Burger number B must be less than unity and the front is perturbed by the return of a portion of the jet when the gyre is fully developed, leading the jet to impinge on the wall related to

(a)

(b)

Figure 15

Comparison between the velocity fields of (a) the reference simulation of Speich (1992) (B ≈ 0.8) at 25 days and (b) the experimental flow (run 9, B ≈ 0.8) at 100 days.

the Spanish coast. These conditions and the diameter of the vortices, ~ O (internal radius of deformation r) permit us to believe than they are generated by baroclinic instabilities. Both in the numerical simulation and in the experiments, the cyclonic vortices are transported by the Atlantic current. Speich (1992) noticed that these structures have an important effect on the destabilizing of the coastal current along the wall related to the African coast, downstream of the western gyre. She estimates that this phenomenon induces the formation of the observed eastern gyre. In the experiments, the vortices are not large and strong enough to destabilize the coastal current. Moreover, as shown on the graphs of Figure 6, a large meander related to the eastern gyre can form while no cyclonic vortices have been noticed. Finally, an anticyclonic circulation develops in the dense water under the gyre, in both models. The reason for this motion is not well understood. We can argue that it is induced by the stress at the interface between the two layers, and that it propagates to the whole layer by spin-down. This explanation is somewhat speculative, because precise measurements of the velocity field in the lower layer are difficult to perform. Moreover, the circulation of the WMDW in the Alboran Sea has yet to be clearly evidenced.

The role of the Alboran Sea is important for the understanding of the hydrodynamics of the Mediterranean Sea because of its position as an "antechamber" of the semi-enclosed sea. By the use of a reduced model, we try to understand the behaviour of its flow pattern. We show the strong influence of the flow regime of the strait, and the deterministic response of the Alboran Sea flow to this regime. However, the flow is more complex. The reason why the gyre may disappear is not understood. Perhaps an answer could be found by considering local and sub-synoptic meteorological conditions. The behaviour and the influence of the Levantine Intermediate Water also need further investigation. Finally, future models will probably have to represent the bottom topography and a more realistic coastal configuration.

Acknowledgements

REFERENCES

Agui J.C., J. Jimenez (1987). On the performance of particle tracking, J. Fluid Mech. 185, 447-468.

Besiktepe S., T. Oguz, H.I. Sur (1990). The upper layer circulation in the sea of Marmara as inferred from the hydrographic data, Rapport de la Commission Internationale pour l'Exploration de la mer Méditerranée (CIESM), 32, 157.

Bormans K.M., C. Garrett (1989). A simple criterion for Gyre formation by the surface outflow from a strait, with application to the Alboran Sea, J. Geophys. Res. 94, 12637-12640.

Conlon D.M. (1983). On the outflow modes of the Tsugaru warm current, La Mer 20, 60-64.

Chabert d'Hières G., H. Didelle, D. Obaton (1991). A laboratory study of surface boundary currents: Application to the Algerian current, J. Geophys. Res. 96, C7, 12539-12548.

Cheney R.E., R.A. Doblar (1982). Structure and variability of the Alboran Sea frontal system, J. Geophys. Res. 87, 585-594.

Gascard J.C., C. Richez (1985). Water masses and circulation in the Western Alboran Sea and in the Strait of Gibraltar, Prog. Oceanogr. 15, 157-216.

Gleizon P. (1994). Étude expérimentale de la formation et de la stabilité de tourbillons anticycloniques engendrés par un courant barocline issu d'un détroit. Application à la mer d'Alboran, Thèse d'Université de Grenoble I, 240 p.

Heburn G.W., P.E. La Violette (1990). Variations in the structure of the anticyclonic Gyres found in the Alboran Sea, J. Geophys. Res., 95, 1599-1613.

Klinger B.A. (1996). Baroclinic eddy generation at a sharp corner in a rotating system, J. Geophys. Res. in press.

Kawasaki Y., T. Sugimoto (1984). Experimental studies on the formation and the degeneration processes of the Tsugaru Warm Gyre, Ocean Hydrodynamics of Japan and East China Seas, J.C.J. Nihoul, ed. Elsevier, Amsterdam, 39, 225-238.

Lanoix F. (1974). Projet Alboran. Étude hydrologique et dynamique de la mer d'Alboran, Rapp. Tech. OTAN 66, 39 p.

Le Vourch J., C. Millot, N. Castagne, P. Le Borgne, J.P. Olry (1992). Atlas des fronts thermiques en mer Méditerranée, d'après l'imagerie satellitaire, Mém. Inst. Océanogr. 16, 146 p.

Madec G. (1990). La formation d'eau profonde et son impact sur la circulation régionale en Méditerranée occidentale : une approche numérique, Thèse de Doctorat de l'Université de Paris VI, 194 p.

Nof D. (1978). On geostrophic adjustment in sea straits and wide estuaries: theory and laboratory experiments. Part II: two-layer system, J. Phys. Oceanogr. 8, 861-872.

Obaton D. (1994). Étude expérimentale de la stabilité d'un courant côtier de gravité. Application au courant algérien, Thèse de Doctorat de l'Université de Grenoble I, 186 p.

Pedlosky J. (1987). Geophysical Fluid Dynamics, Springer Verlag, New York, 710 p.

Perkins H., T. Kinder, P. La Violette (1990). The Atlantic inflow in the Western Alboran Sea, J. Phys. Oceanogr. 20, 242-263.

Preller R., H.E. Hulburt (1982). A reduced gravity model of circulation in the Alboran Sea, in Hydrodynamics of Semi-enclosed Seas, J.C.J. Nihoul, ed. Elsevier, Amsterdam, 34, 75-89.

Speich S, M. Crépon, G. Madec (1996). The circulation of the Alboran Sea: a sensitivity study, J. Phys. Oceanogr. in press.

Speich S. (1992). Étude du forçage de la circulation océanique par les détroits : cas de la mer d'Alboran, Thèse de Doctorat de l'Université de Paris VI, 245 p.

Tintore J., D. Gomis, G. Parilla (1991). Mesoscale dynamics and vertical motion in the Alboran Sea, J. Phys. Oceanogr. 21, 811-823.

Ünlüata Ü., T Oguz., M.A. Latif, E. Özsoy. On the physical oceanography of the Turkish Straits, in: Physical Oceanography of Sea Straits (Series C), L.J. Pratt ed. Kluwer, Dordrecht, 25-60.

Werner F.E., A. Cantos-Figuerola, G. Parrilla (1988). A sensitivity study of reduced-gravity channel flow with application to the Alboran Sea, J. Phys. Oceanogr. 18, 373-383.

Whitehead J.A. (1985). The deflection of a baroclinic jet by a wall in a rotating fluid, J. Fluid Mech. 157, 79-93.

Whitehead J.A., A.R. Miller (1979). Laboratory simulation of the Gyre in the Alboran Sea, J. Geophys. Res. 84, 3733-3742.